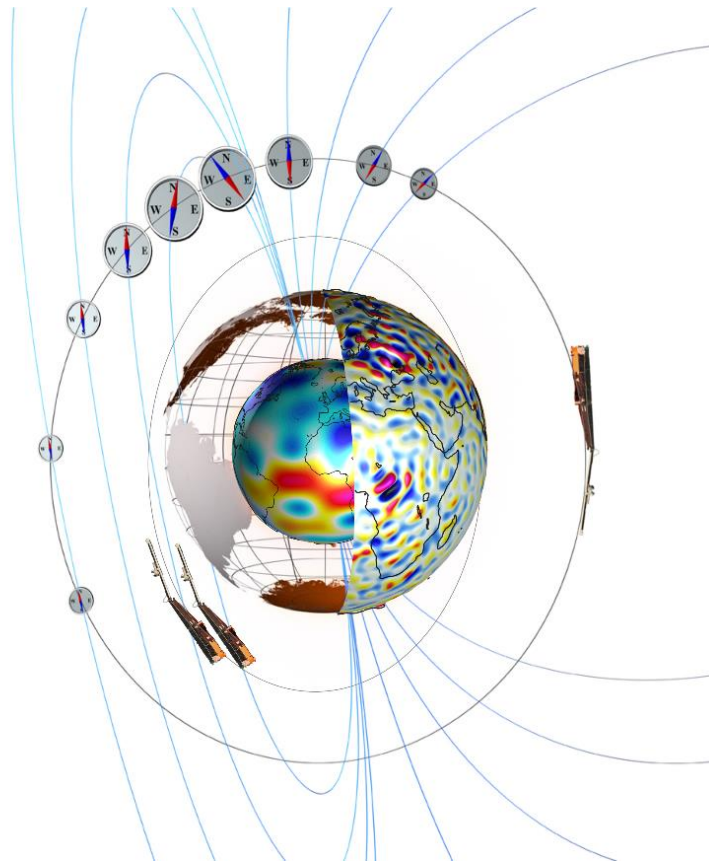


Data, Innovation, and Science Cluster

Review of Swarm L1B data quality



Doc. no: ESA-EOPG-EOEP-TN-24, Rev: 1 dA, 08/05/2020

Prepared:

Approved:

Filomena Catapano, Enkelejda Qamili,

Jerome Bouffard

Christian Siemes

Date 08/05/2020

Swarm Data Quality Manager -ESA

Date 08/05/2020

Swarm Data Quality Team

© <name of your entity, like "DTU Space">, <Country of your entity>, 2020. Proprietary and intellectual rights of <name of your entity, like "DTU Space">, <Country of your entity> are involved in the subject-matter of this material and all manufacturing, reproduction, use, disclosure, and sales rights pertaining to such subject-matter are expressly reserved. This material is submitted for a specific purpose as agreed in writing, and the recipient by accepting this material agrees that this material will not be used, copied, or reproduced in whole or in part nor its contents (or any part thereof) revealed in any manner or to any third party, except own staff, to meet the purpose for which it was submitted and subject to the terms of the written agreement.

Record of Changes

Reason	Description	Rev	Date
Initial vers.	Released	1 dA	08/05/2020

Table of Contents

1	Reference Documents	7
2	Abbreviations	9
3	Introduction.....	12
3.1	Scope and applicability	12
4	ORBATT L1B Data Products	13
4.1	Star Tracker	13
4.1.1	Recent achievements.....	13
4.1.2	Future evolutions.....	13
4.2	GPS receiver	13
5	MAGNET L1B Data Products	14
5.1	ASM-VFM scalar residuals	14
5.2	On-ground magnetic survey	16
5.3	Future investigation and next step.....	18
6	PLASMA L1B Data Products	19
6.1	Characterization of the EFI-LP data quality	19
6.1.1	Dependence on the solar activity	20
6.1.2	Dependence on the local time.....	23
6.1.3	Dependence on the geomagnetic location.....	25
6.2	New baseline achievements	27
6.2.1	New LP product interpolated at exact UTC	27
6.2.2	Te computed from high gain probe	28
6.3	Recent tests performed on the LPs	30
6.3.1	Both probes set in high/high gain.....	30
6.3.2	Swap of LP gain setting	31
6.4	On-going investigations and expected improvements.....	32
6.4.1	Extreme values of the electron temperature	32
6.4.2	LP difference	32
6.4.3	Hick-ups	33
6.4.4	Ne fluctuations.....	33
7	ACCELE L1B Data Products.....	34
7.1	Temperature-induced bias variations.....	34

7.2	Sudden changes of the bias (steps)	35
7.3	Slow changes of the bias (silent steps)	36
7.4	Autonomous reboot of the accelerometer.....	37
7.5	Sudden changes in sensitivity	37
7.6	Pink noise	37
7.7	Non-unit scale factors	38
7.8	Spikes	40
7.9	Harmonic perturbations.....	41
7.10	Polarization voltage perturbations	42
7.11	Coupling between accelerometer axes.....	44
7.12	Summary and perspective	44

1 Reference Documents

The following documents contain supporting and background information to be taken into account during the activities specified within this document.

- [RD.1] <https://earth.esa.int/documents/10174/1514862/Swarm-Level-1B-baseline-evolutions>
- [RD.2] <https://earth.esa.int/web/guest/missions/esa-eo-missions/swarm/instruments-overview>
- [RD.3] https://earth.esa.int/documents/10174/1514862/Swarm_Level-1b_Processor_Algorithms
- [RD.4] <https://earth.esa.int/web/guest/swarm/data-access/quality-of-swarm-l1b-l2cat2-products>
- [RD.5] M. Herceg, P.S. Jørgensen, J.L. Jørgensen (2017) Characterization and compensation of thermo-elastic instability of SWARM optical bench on micro Advanced Stellar Compass attitude observations. *Acta Astronautica*, 137, 205-213, ISSN 0094-5765, <https://doi.org/10.1016/j.actaastro.2017.04.018>.
- [RD.6] G. Allende-Alba, O. Montenbruck, A. Jäggi, D. Arnold, F. Zamgerl (2017) Reduced-dynamic and kinematic baseline determination for the Swarm mission. *GPS Solutions* July 2017, Volume 21, Issue 3, pp 1275–1284. <https://doi.org/10.1007/s10291-017-0611-z>
- [RD.7] Jose van den IJssel, B. Forte, O. Montenbruck (2016) Impact of Swarm GPS receiver updates on POD performance. *Earth, Planets and Space*, 68:85. <https://doi.org/10.1186/s40623-016-0459-4>
- [RD.8] Finlay, C.C., Kloss, C., Olsen, N., Hammer, M. and Tøffner-Clausen, L., (2019) DTU Candidate models for IGRF-13. Technical Note submitted to IGRF-13 task force
- [RD.9] Tøffner-Clausen, L., Lesur, V., Olsen, N. et al. In-flight scalar calibration and characterisation of the Swarm magnetometry package. *Earth Planet Sp* 68, 129 (2016). <https://doi.org/10.1186/s40623-016-0501-6>
- [RD.10] https://earth.esa.int/documents/10174/1514862/Swarm_L1b_Product_Definition
- [RD.11] <https://earth.esa.int/documents/10174/1514862/swarm-level-1B-plasma-processor-algorithm.pdf>
- [RD.12] Knudsen, D. J., J. K. Burchill, S. C. Buchert, A. I. Eriksson, R. Gill, J.-E. Wahlund, L. Åhlen, M. Smith, and B. Moffat (2017), Thermal ion imagers and Langmuir probes in the Swarm electric field instruments, *J. Geophys. Res. Space Physics*, 122, 2655–2673, doi:10.1002/2016JA022571
- [RD.13] <https://swarm-diss.eo.esa.int/>
- [RD.14] <https://www.swpc.noaa.gov/phenomena/f107-cm-radio-emissions>
- [RD.15] Kelley, M. C., *The earth's ionosphere : plasma physics and electrodynamics*, Second Edition, INTERNATIONAL GEOPHYSICS SERIES vol 96, Elsevier.
- [RD.16] http://wdc.kugi.kyoto-u.ac.jp/dst_realtime/201907/index.html
- [RD.17] Archer, W. E., Gallardo-Lacourt, B., Perry, G. W., St.-Maurice, J.-P., Buchert, S. C., & Donovan, E. F. (2019). Steve: The optical signature of intense subauroral ion drifts. *Geophysical Research Letters*, 46, 6279– 6286. <https://doi.org/10.1029/2019GL082687>
- [RD.18] Swarm Accelerometer Anomaly Report, SW-RP-VZLU-GS-002, Rev 1dA, 2014-10-20.

[RD.19] Calibration of Swarm accelerometer scale factors, SWAM-GSEG-EOPG-TN-15-0008, Issue 1, Rev 0, 13/04/2015.

2 Abbreviations

A list of acronyms and abbreviations used by Swarm partners can be found below..

<i>Acronym or abbreviation</i>	<i>Description</i>
ACC	Accelerometer
ACCELE	Operational Level 1b Processor of ACC data
ASM	Absolute Scalar Magnetometer
CCDB	Characterisation and Calibration Database
CHAOS	High-precision magnetic Field model derived by DTU Space
CHU	Camera Head Unit
dB_Sun	Sun induced stray field
DISC (Swarm)	Data, Innovation, and Science Cluster
Dst	Disturbance storm time index
DTU	Technical University of Denmark (DK)
DTU-MI	DTU Space, division of Measurement and Instrumentation
DUT	Delft University of Technology (NL)
EFI	Electrical Field Instrument, including the TII and the LP
EO	Earth Observation (ESA)
ESA	European Space Agency
FP	Faceplate
IBA	Inter Boresight Angle
ICRF	International Celestial Reference Frame
IGRF	International Geomagnetic Reference Field
IS radar	Incoherent Scatter radar
ITRF	International Terrestrial Reference Frame
L1B	Level 1B (satellite data)
L1BOP	Level 1B Operational Processor
L2	Level 2 (satellite data)
LEO	Low Earth Orbit
LP	Langmuir Probe, part of the Electrical Field Instrument
MAGNET	Operational Level 1B Magnetic processor
MLT	Magnetic Local Time
MMEG	Magnetic Measurement Expert Group

Acronym or abbreviation	Description
NEC	North, East, Center coordinate system
OP	Operational Processor
OPER	Operational data (nominal)
ORBATT	Operational Level 1B orbit and attitude processor
PLASMA	Operational Level 1B Plasma processor
POD	Precise Orbit Determination
PP	Prototype Processor
QC	Quality Control
QD	Quasi-Dipole
SH	Spherical Harmonics
STR	Star Tracker
TII	Thermal Ion Imager, part of the Electrical Field Instrument
VFM	Vector Field Magnetometer

Table of Figures

Figure 3-1 :	14
Figure 3-2 :	16
Figure 3-3 :	17
Figure 3-4 :	18
Figure 4-1 :	21
Figure 4-2 :	22
Figure 4-3 :	23
Figure 4-4 :	24
Figure 4-5 :	26
Figure 4-6 :	27
Figure 4-7 :	28
Figure 4-8 :	29
Figure 4-9 :	30
Figure 4-10 :	31
Figure 4-11 :	32
Figure 5-1:	35
Figure 5-2:	36
Figure 5-3:	36
Figure 5-4:	37
Figure 5-5:	38
Figure 5-6:	39
Figure 5-7:	40
Figure 5-8:	41
Figure 5-9:	41
Figure 5-10:	42
Figure 5-11:	43
Figure 5-12:	43
Figure 5-13:	44

Table of Tables

Table 1: Scale factors estimated from dedicated satellite manoeuvres.	40
--	----

3 Introduction

3.1 Scope and applicability

This document is a review of the L1B data quality status after the full reprocessing performed in September 2018 [RD.1]. It is worth to specify that the L1B processor comprises of four individual processors, that are the ORBATT, MAGNET, ACCELE, and PLASMA. The ORBATT processor mainly generates attitude and orbit information data products, measured from GPS and Star Tracker (STR) instruments. The MAGNET processor generates data products measured from the Vector Field Magnetometer (VFM) and Absolute Scalar Magnetometer (ASM) instruments. The ACCELE products are measured from the Accelerometer (ACC) instrument, while the PLASMA products are measured from the Langmuir Probe (LP) instrument, which is part of the Electric Field Instrument (EFI). For more information on the instruments on board Swarm we refer to [RD.2]. The quality monitoring techniques together with a statistical characterization of the latest baseline data quality, are discussed in detail in this document for Swarm L1B data products.

4 ORBATT L1B Data Products

4.1 Star Tracker

Each of the three Swarm satellites is equipped with three micro Advanced Stellar Compass Camera Head Units (CHU) mounted on a common optical bench (OB), which has a purpose of transference of the attitude from the star trackers to the magnetometer measurements. Such instrument on board Swarm Alpha, Bravo and Charlie operates nominally ([RD.1]), delivering high-quality pointing data at 1 or 2 Hz (see next).

4.1.1 Recent achievements

From tests performed on-ground, an improvement of the performance of STR pointing measurements has been observed by using a data rate of 2Hz. As a consequence, an increase of STR frequency from 1 Hz to 2 Hz was introduced for Swarm Alpha on 12/12/2018, for Swarm Bravo on 17/10/2018 and for Swarm Charlie on 18/12/2018. After such modification an update of STR_q_CHU CCDB files (see [RD.3]) was introduced in L1B processing chain. This change was needed to bring the CHU frames after the switch to 2Hz into the CHU frames before the switch (i.e. no Euler Angle update was needed).

The only known issue present in STR data is an anomalous variation (up to ~ 0.85 arc-sec/ $^{\circ}$ C) in the STR Inter Boresight Angle (IBA) for Camera Head Unit (CHU) pairs. A STR correction model that uses as input CHU and optical bench temperatures have been proposed by the instrument manufacturers. After an extensive validation process it has been decided to include this model in the L1B algorithm and new operational processing baseline, data with Product Baseline and File Counter 0401. The baseline numbers are the last four numerical digits in the Swarm product file name extensions, and actually represent the file version [RD.4]. This model allows pre-flight and in-flight IBA measurements to match mostly within arc-seconds for Alpha and Charlie, and with a bit higher offsets for Bravo. An improvement (> 10 arc-seconds) of the STR attitudes accuracy is therefore also observed. More details in [RD.5].

4.1.2 Future evolutions

Since March 2018, the STR instruments on-board of the three Swarm spacecraft is operating as particle detector (through counting of hotspots). The first results are very promising, e.g., clear day and night and east and west flux differences are observed. Further analyses are on-going. As soon as a consolidated processing procedure is set-up, the generation of particle flux will be implemented in L1B data processing chain.

4.2 GPS receiver

GPS receiver measurements were analysed in detail in the scientific literature. The reader can refer to [RD.6] and [RD.7] for more details on the GPS receiver performance and assessments.

5 MAGNET L1B Data Products

The Swarm Magnetic field Level 1B data contains the fully calibrated and corrected vector and scalar magnetic field measurements. The magnetic field data, currently with product baseline and file counter 0506, are used to generate reference magnetic field models of internal and external origin (i.e. Swarm L2 products and other models) confirming the excellent health of Magnetic package instruments and the very high quality of such data [RD.8].

5.1 ASM-VFM scalar residuals

As described in previous technical reports and papers ([RD.4]and references therein), early in the Swarm mission it was recognised that the measurements from the two magnetometer instruments (ASM and VFM) on-board each spacecraft measure slightly different absolute magnetic field values. This effect has been analysed and interpreted as a magnetic disturbance of varying strength and direction. It was observed that such disturbance was highly correlated with the Sun incident angle with respect to the spacecraft. Thanks to the joint effort of a Magnetic Measurements Expert Group (MMEG) an empirical correction model was established based on in-depth analyses of instrument and housekeeping data. In this model, the Sun induced magnetic disturbance vector is described by three spherical harmonic expansions (of degree 25), one for each field component, parameterised by the Sun incident angles on the spacecraft, denoted α and β (see Figure 5-1) (a detailed description of this correction model can be found in [RD.9]).

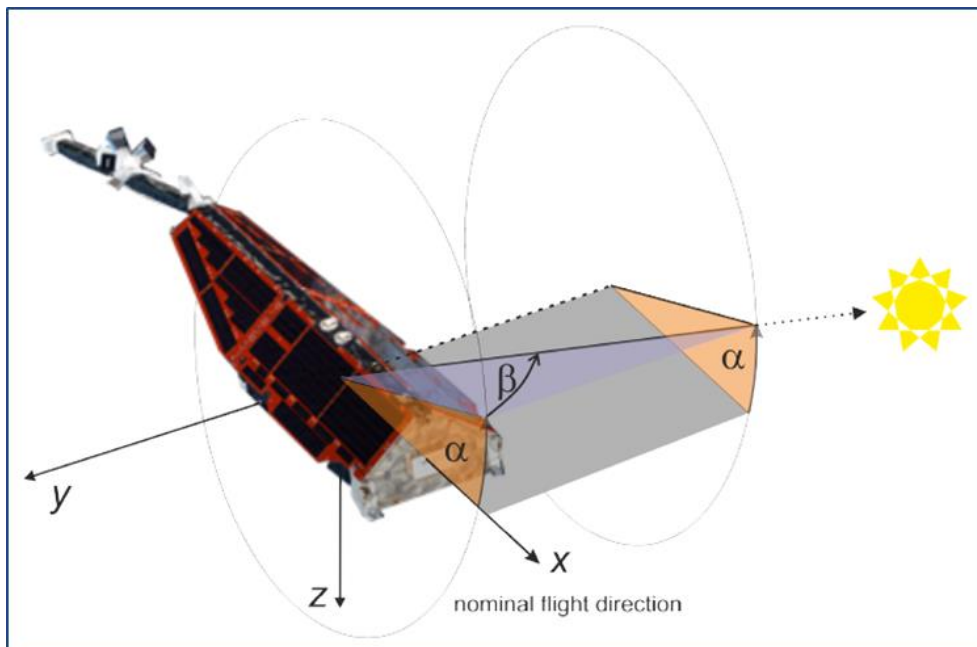


Figure 5-1 :
Illustration of Sun incident angles, α and β .

After an extensive validation process finalised in July 2015, it was decided to include this model in the L1B MAGNET algorithm introducing a new operational processing baseline. This disturbance model was considered as a stray field vector at the VFM instrument location only and was stored in the following magnetic products: MAGx_HR_1B, MAGx_LR_1B and MAGx_CA_1B [RD.10]. It is worth to specify that the variable dB_Sun (see [RD.3]) is not independently characterized, i.e., it is co-estimated together with a model of the temporal evolution of the VFM sensitivity and an adjustment of the pre-flight estimated non-orthogonality angles of the VFM sensor. In such a way, the users had no access to the so-called “Original” residuals, i.e., the differences between ASM scalar field and the modulus of VFM data calibrated with only pre-flight calibration parameters. In September 2018 a second modification was therefore introduced in the L1B MAGNET processing algorithms, consisting in a clear separation of the pre-flight and the inflight VFM calibration parameters. In this way, the users have access to the parameter B_pre (see [RD.3]) which is stored in MAGx_CA_1B products as a source of “original residuals”.

The introduction of the dB_Sun correction model decreased the differences between ASM and VFM data significantly for the whole mission period, as shown in the Figure 5-2. Indeed, the weighted rms of the scalar residuals reduces from 1.19 nT to 255 pT for Swarm Alpha (see Figure 5-2 upper panel) and from 822 pT to 219 pT for Swarm Bravo (see Figure 5-2 bottom panel).

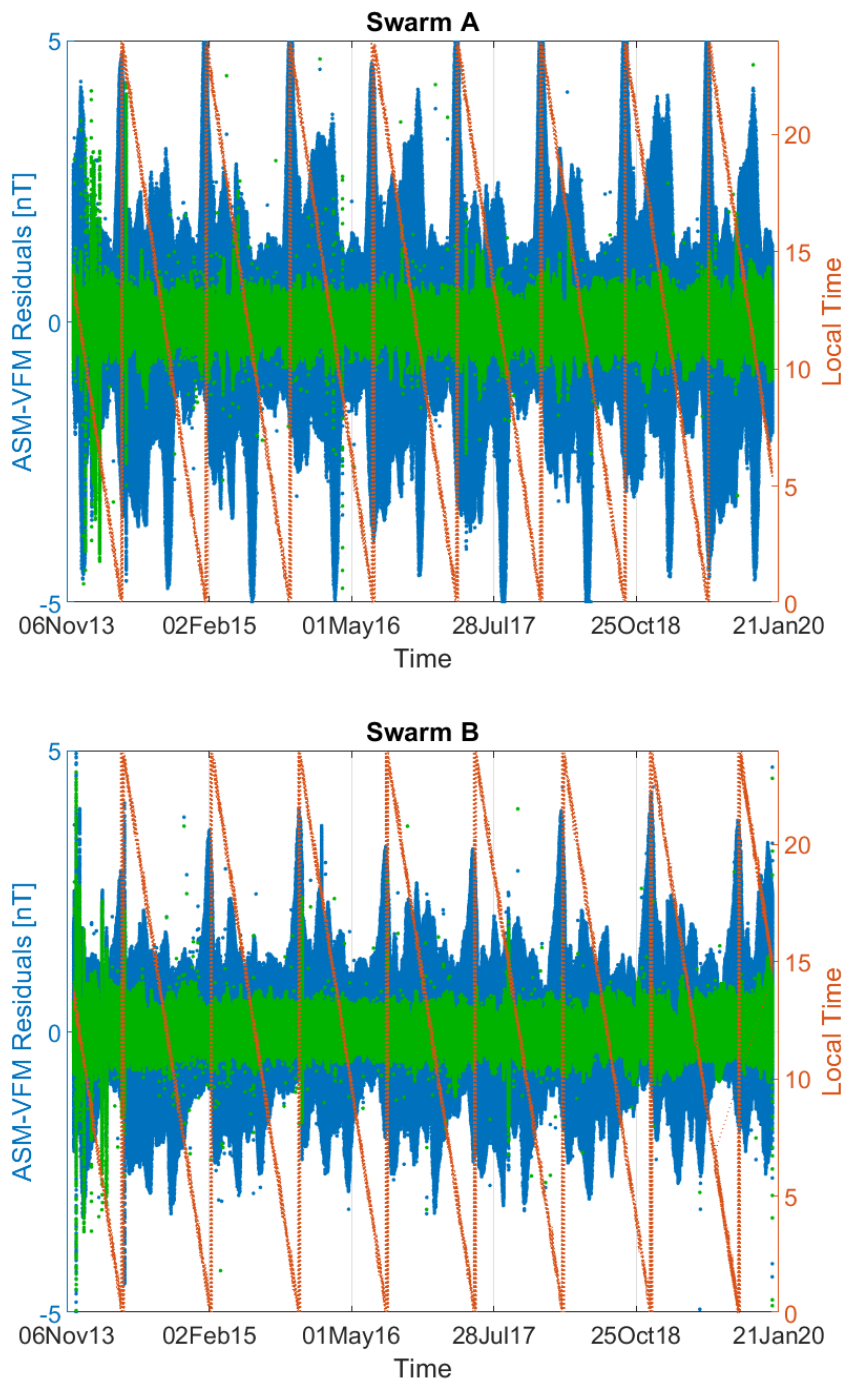


Figure 5-2 :

Scalar residuals of uncorrected (blue) and corrected (green) measurements as a function of time. Local time of the ascending node is shown in red (right axis).

5.2 On-ground magnetic survey

Although the operational dB_Sun correction model is performing very well, the MMEG continues to further investigate the root-cause of such disturbance. In this respect, a thorough on-ground magnetic survey of the materials around the VFM sensor has been performed. Since the perturbation seemed to be induced by solar heat flux (see previous section), on-ground experiments were focused on the analysis of thermoelectric cur-

rents. From the obtained results, it follows that the observed perturbation is likely due to a thermoelectric current flowing in the MLI blanket of VFM instrument and returning through the grounding network that is needed to prevent the build-up of static electricity.

In the current Swarm configuration, the grounding is done at two rivets on the blanket that are placed at different locations of the VFM blanket (see Figure 5-3) resulting in different view factors to the sun. Thus, a temperature difference (ΔT) between the two rivets is expected as the satellites scan different sun impingements during the flight. Based on that, it is theoretically possible to model the temperature difference of the two rivets function of sun incident angles, calculate the corresponding thermoelectric current, and then estimate the perturbation on the VFM sensor.

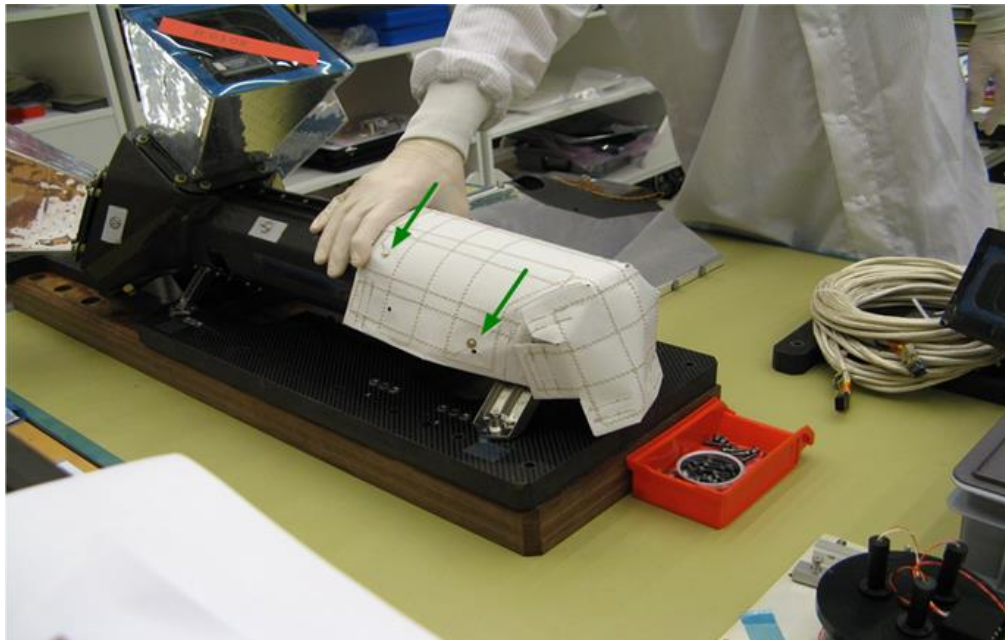


Figure 5-3 :

Aluminium rivets used as grounding terminals of the VFM blanket to the grounding network (Picture courtesy of DTU).

Another very interesting outcome from this on-ground analysis is that not only the VFM instrument but also the ASM instrument (located at the tip of the spacecraft boom) is probably also affected by such disturbance. The blanket near the ASM sensor has a geometry that could generate perturbation from thermoelectric currents between two rivets (see Figure 5-4). The analysis of the blanket verifies that the empirical disturbance vector in y-axis can originate from this blanket and perturb the ASM.



Figure 5-4 :

Rivets used as grounding terminals of the ASM blanket to the grounding network (Picture courtesy of AIR-BUS).

5.3 Future investigation and next steps

The MMEG is working to build a physical based dB_Sun correction model considering all the outcomes from tests performed on-ground. This new physics-based correction model will consist in two different models, one for the VFM instrument (disturbed in all the three directions, X, Y and Z) and another one for the ASM instrument (disturbed almost exclusively in the Y (East-West) direction). The latter has minor impact on the ASM scalar measurements during nominal flight. For this reason, the expert team is also taking advantages of some periods when Swarm spacecraft was flying not in the nominal direction (i.e., during manoeuvres) in order to better characterise the disturbance induced at the ASM instrument.

Linked to this activity, there is another on-going investigation performed by Romanian Academy which aims at simulating the magnetic field induced by the thermal blanket configuration at the ASM location by considering the properties and geometry of the thermal blanket and grounding wiring configuration. The first outcome of this study confirms that there is a preferred direction for the magnetic field disturbance at the ASM location in the Y-direction.

The MMEG has already proposed a physics-based compensation model for the VFM and an empirical ASM compensation models for the Swarm Alpha and Bravo. First results are encouraging but more work needs to be done before an operational implementation in a future Swarm processing baseline.

6 PLASMA L1B Data Products

The Electric Field Instrument (EFI) consists of two components: the Langmuir Probes (LPs) and the Thermal Ion Imager (TII). This document only refers to the LP data products as the TII processing is outside the scope of an automated Level 1B processor, because the TII derived products are considered as an experimental dataset [RD.4]. The LPs provide estimates of the density (Ne) and electron temperature (Te) of the plasma surrounding the satellite, as well as the electric potential of the spacecraft (Vs).

The probes consist in two spheres mounted on about 10 cm long stubs at the Earth-facing front part of the satellites. Each Swarm satellites is carrying two probes: Probe 1 is on the bottom left side of the satellite, it is currently set in high gain and is made of nitrated titanium (TiN); Probe 2 is on the bottom right side, it is currently set in low gain and is covered with gold (Au). The electronic design of the Swarm LPs alternates between two sub-modes, the classical sweep and the harmonic sub-mode (HM). During the sweep mode, the current between the probe and the satellite is measured by varying the probe bias in small steps over the complete range of values that could possibly be relevant. For the HM, by tracking a specific current on board, only three bias points are selected at values which are most relevant for determining plasma parameters. At these points the bias voltage is modulated with a small amplitude harmonic signal to measure the current and admittances.

The sweep mode is done only once every 128s for a duration of 1s, while the HM is performed for more than 99% of the time at three specific point of the current-voltage characteristic curve. At each point the “rippling” lasts for about 100 ms, and the current and admittance are averaged over roughly ten ripple cycles. The variables Ne, Te and Vs are estimated via the HM at 2Hz rate. For more details we remand to [RD.11] and [RD.12].

Since the full reprocessing [RD.1], the algorithm to compute the EFlx_LP_1B data has been largely improved. For example, the variables Ne and Te are computed mainly from the Probe set in high gain. In the past high and low gain probes gave systematically different Te, particularly at night times. The low gain Te is up to many hundred K higher. Comparison with models and Incoherent Scatter radar data showed that the high gain Te seemed closer to reality. On the opposite, the Vs is computed mainly from the Probe set in low gain, while in the previous version of the processor the measurements from the high and low gain were blended together for the computation of all the variables. A systematic difference between the measures in HM and sweep mode were also observed. Thus the L1B products are currently derived only from data in HM to avoid discontinuities in the data products.

In the following sections, the L1B data quality of the LPs measurements is assessed and statistical analysis are performed. Also, the data monitoring techniques are described together with the investigations performed to gain a better understanding of the anomalies affecting the data products.

6.1 Characterization of the EFI-LP data quality

The EFlx_LP_1B product contains plasma data from the LPs of the EFI. The plasma product encompasses the plasma density, electron temperature, and spacecraft potential. Currently, two plasma products are available in the Swarm dissemination server [RD.13]: one at LP timestamp (EFlx_LP_1B) and the other one interpolated to full UTC seconds (EFlxLPI_1B). Both products contain exactly the same variables and the same characteristics [RD.11]. In the following results of an analysis characterizing the Swarm EFlx_LP_1B data quality are reported. In order to have an easier visualization and to avoid redundancy of information, the results are shown for only one of the three spacecraft unless there are differences among the three.

6.1.1 Dependence on the solar activity

By performing a statistical analysis of the data (from January 2014 to June 2019) it is well visible that the plasma parameters depend strongly on the solar activity. Figure 6-1 shows the daily average of the density and electron temperature (red squares in panels (a) and (b), respectively) together with the temporal standard deviation (vertical bars) measured on board Swarm Alpha, while the panel (c) shows the daily F10.7 solar radio flux index. F10.7 is a proxy for the solar EUV flux which is the dominating source of ionization, molecular dissoziation, and heat in the thermosphere-ionosphere [RD.14]. From a visual analysis it is clear that Ne and the F10.7 index are correlated; indeed during strong solar activity, when F10.7 reaches higher values, also the density is higher. On the contrary, the electron temperature generally decreases when the solar activity is stronger. This is a typical behaviour of the ionospheric plasma variables with respect to the solar cycle variation [RD.15]. In particular for the Swarm data, the correlation coefficient between density and F10.7 index results to be equal to $R = 0.79 \pm 0.02$, suggesting a linear correlation between the two variables. While, the correlation coefficient between the electron temperature and F10.7 index results to be $R = -0.21 \pm 0.04$, indicating a weak anti-correlation.

It is worth to notice that, in correspondence of strong geomagnetic storms, the standard deviation of the density is larger. For example, by considering the years when the solar activity was more intense as the 2014 and 2015, we can see very large standard deviation corresponding to intense fluctuations of the density related to the geomagnetic disturbances. When the solar activity is less intense, also the standard deviation becomes smaller. As expected, the opposite behaviour is observed for the standard deviation of the electron temperature. Superimposed is a periodic variation of mean values and standard deviation as a result of the regression of the orbital plane in local time. The orbital plane moves from noon-midnight to dawn-dusk and back to noon-midnight in about 140 days corresponding to the periodic variations seen in Figure 6-1. These results are useful to get a measure of the good quality of the Swarm LP data products.

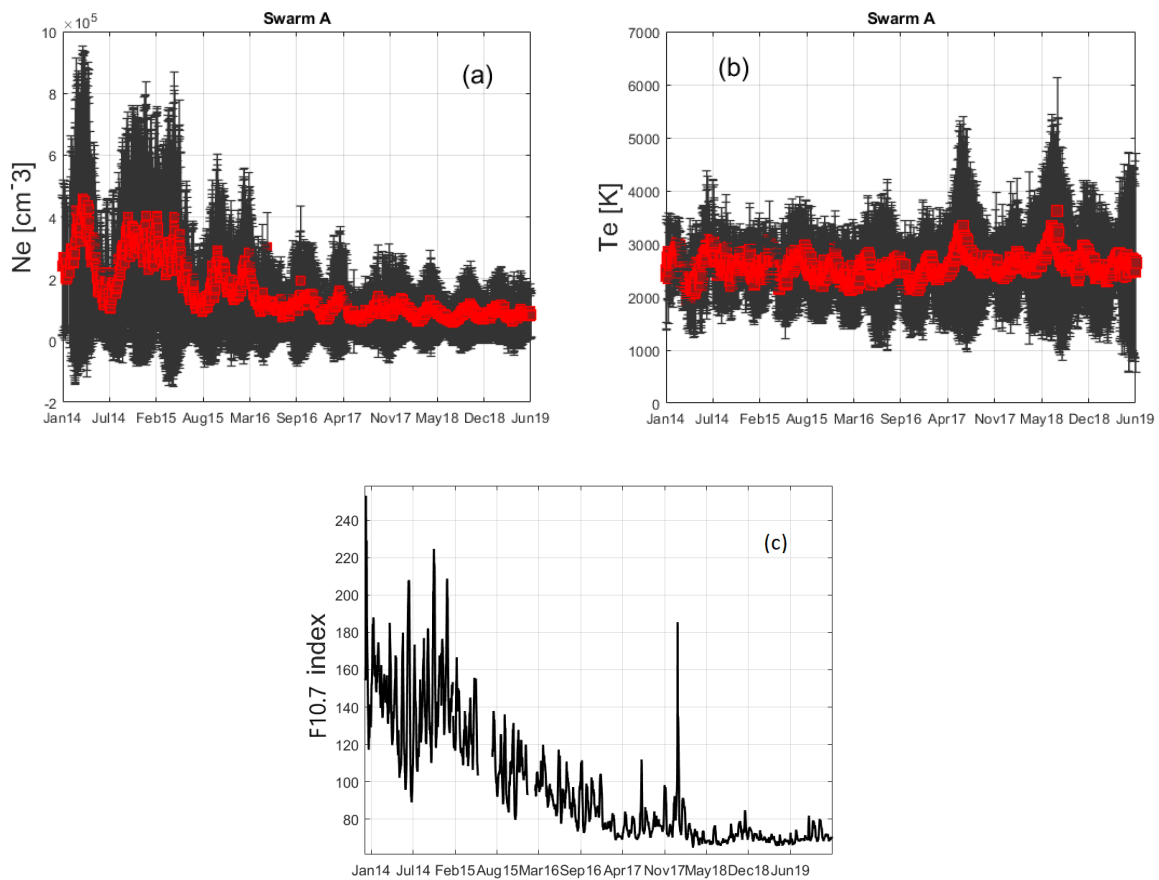


Figure 6-1 :

Daily average (red squares) and standard deviation (vertical bars) of the density (a) and electron temperature (b) measured on board Swarm Alpha from the 1st of January 2014 to the 30th of June 2019. Panel (c) shows the variation of the F10.7 index in the same time period.

To assess the quality of data, it is possible to consider the percentage of flagged values. The Flags are used to relate a potential error in the data with its source. Therefore, for some specific flag values it is recommended to discard the data (see Table 6-4 and 6-5 in [RD.10]). Figure 6-2 shows the daily and monthly average of the percentage of flagged values for the density and the electron temperature measured on board Swarm Bravo between July 2014 and June 2019. As expected, for the density the percentage of flagged values increase as the solar activity decreases, while the inverse variation is observed for the electron temperature. It is well known that during the solar minimum, the electron density in the ionosphere is lower, mainly due to the less intense ionizing solar ultraviolet [RD.15]. The temperature is intuitively lower near solar maximum, because the electron cooling rates are larger owing to the high density. The flags for the EFlx_LP_1B data [RD.10], are also used to identify non-physical values, as for example negative values of density or electron temperature. Almost all flags of densities are caused by negative values. During the minimum of the solar cycle the density is lower, as a consequence negative density values are measured more often and are flagged. Thus, during the solar minimum the percentage of flagged density values increases, due to the frequent measured negative values. Once again, the opposite behaviour is observed for the electron temperature, where more flagged values occur near solar maximum. Flagged Te is often (but not always) caused by overflow in the ADC, because the more sensitive high-gain probe is used. The high density produces high currents which let the ADC overflow. The correlation between the F10.7 index and the percentage of flagged Te results to be $R = 0.71 \pm 0.02$, thus the two variables are linearly correlated. While it is difficult to evaluate a correlation coefficient between the density and F10.7 index because of the percentage of flagged values is often equal to zero.

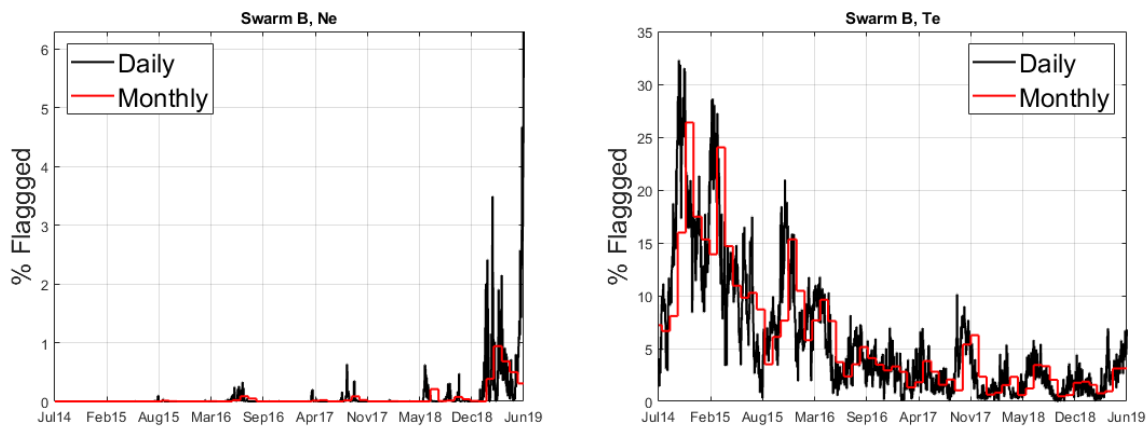


Figure 6-2 :

Daily and monthly percentage of flagged values (black and red lines, respectively) for density and electron temperature (left and right panel, respectively) measured on board Swarm Bravo between 1st of July 2014 and 30th of June 2019.

Figure 6-3 shows a comparison of a daily time series of the electron density measured on board Swarm Bravo during the 26th of February 2015 (left panel), thus during the maximum of the solar cycle, and during the same day of the year 2019 (right panel), thus in the solar minimum. By comparing the two panels it is visible that the occurrence of negative values is very frequent during the solar minimum, while negative density is not measured during solar maximum. In order to compare the measurements in those two days, the dataset has not been filtered by removing flagged values. The local time for the data in the 2015 was of 11 am - 23 pm, while in 2019 was of 6 am – 18 pm. The percentage of flagged values is of the 1.3% for the day in 2019 and zero in 2015. The result has not dependence on the local time, indeed, as shown in Figure 6-2 left panel, in the 2015 the percentage of flagged values is zero, while in 2019 reaches peak of 3% in one month. These results demonstrate the good quality of the EFI-LP data, reflecting the relation of ionospheric variation with respect to the solar activity, and the utility of the flags monitoring as a proxy to characterize the data quality status.

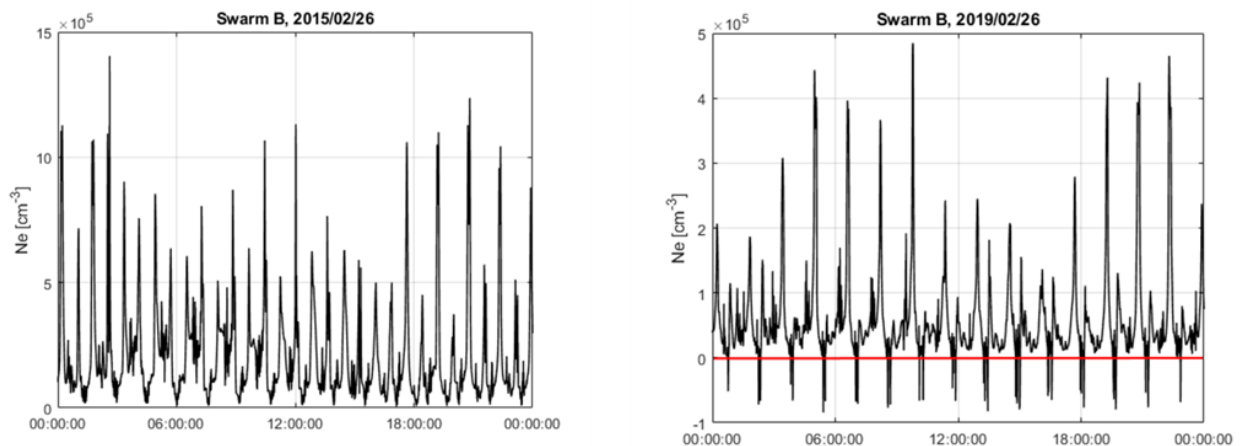


Figure 6-3 :

Density measured on board Swarm Bravo during the 26th of February 2015 and same day in 2019 (left and right panel , respectively). The horizontal red line denotes the value of density equal to zero.

6.1.2 Dependence on the local time

The panels in Figure 6-4 contain several information on the variability of the EFix_LP_1B data products with respect to the local time. The Figure 6-4 shows the daily average of density and the electron temperature measured by separating the ascending and descending phase of the orbits. Data are measured on board Swarm Charlie between January 2015 and December 2016. The period has been chosen to include the geomagnetic storm occurred on the 17th of March 2015, together with quiet periods. Additionally, this time window has been chosen in order to analyse all the possible local time explored by the spacecraft.

Considering the noon-midnight orbits (see right axis for reference), the average values of the density is almost the same for ascending and descending orbits. This feature is not observed during March 2015, probably due to the occurrence of the very strong geomagnetic storm (St. Patrick's storm) having a minimum of Dst index around -222 nT on the 17th of March.

Considering the dawn-dusk orbits, which are between the vertical dashed lines, it is possible to observe that the electron density is higher for the part of the orbit crossing the equator at noon. These results alternate between ascending and descending phases, due to the drifting orbit of Swarm satellites.

This analysis shows that Swarm data are capable to describe the main characteristics of the ionosphere variability with respect to the local time.

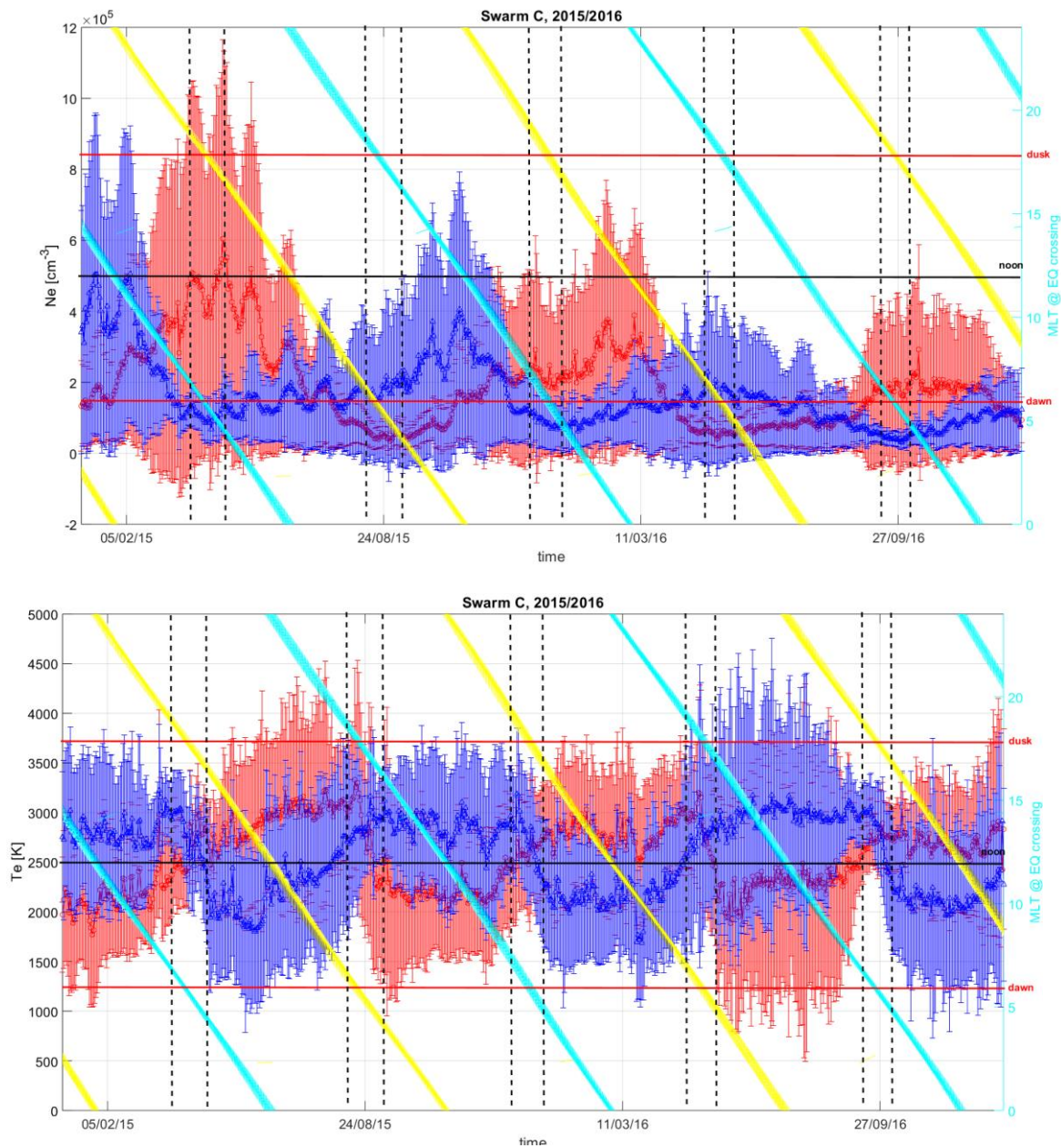


Figure 6-4 :

Daily average (circles) and standard deviation (vertical bars) of density and electron temperature (upper and bottom panel, respectively) measured on board Swarm Charlie in the years 2015 and 2016.

The data are separated between ascending and descending (red and blue marks) orbit phases. The diagonal lines represent the local time of the spacecraft at the equatorial crossing during ascending (yellow) and descending (cyan) phase of the orbit (see right vertical axis for reference). The horizontal lines guide the eye to recognize the local time at noon (black), dawn and dusk (red), while the dashed vertical lines denote the dawn-dusk orbit types.

6.1.3 Dependence on the geomagnetic location

LPs on board Swarm, can well capture the ionospheric variability in short intervals of time. Figure 6-5 shows the variation of Ne and Te as a function of time and Latitude in quasi dipole coordinate system. The figure shows data measured on board Swarm Bravo between the 8th and the 15th of March 2018. The lateral vertical panel shows the average for each degree in latitude together with the standard deviation.

An interesting feature, is the typical double peak of the electron density at equatorial latitudes. This effect is related to the equatorial fountain [RD.15], and is well captured by the Swarm measurements mainly in the day-side. At mid to low latitudes the density is higher, showing two peaks at around 10-15 deg in latitude, and slightly lower values at equator. Then, moving to higher latitudes, the density is lower again.

The electron temperature instead, presents a different feature showing lower values at mid- and low- latitudes, and higher values at higher latitudes. This is another typical characteristic of ionospheric plasma. The narrow peak of Te near ± 60 deg latitude is probably a feature of the nightside ionospheric trough associated with channels of fast plasma flow and the Steve aurora.

The same kind of features are also visible in Figure 6-6, showing a Lat-Long map of Swarm Alpha measurements during the 10th of September 2019. It is possible to observe the opposite behaviour of Ne and Te with respect to the Latitude. In particular, the density being higher at lower latitudes, and the temperature being higher at higher latitudes.

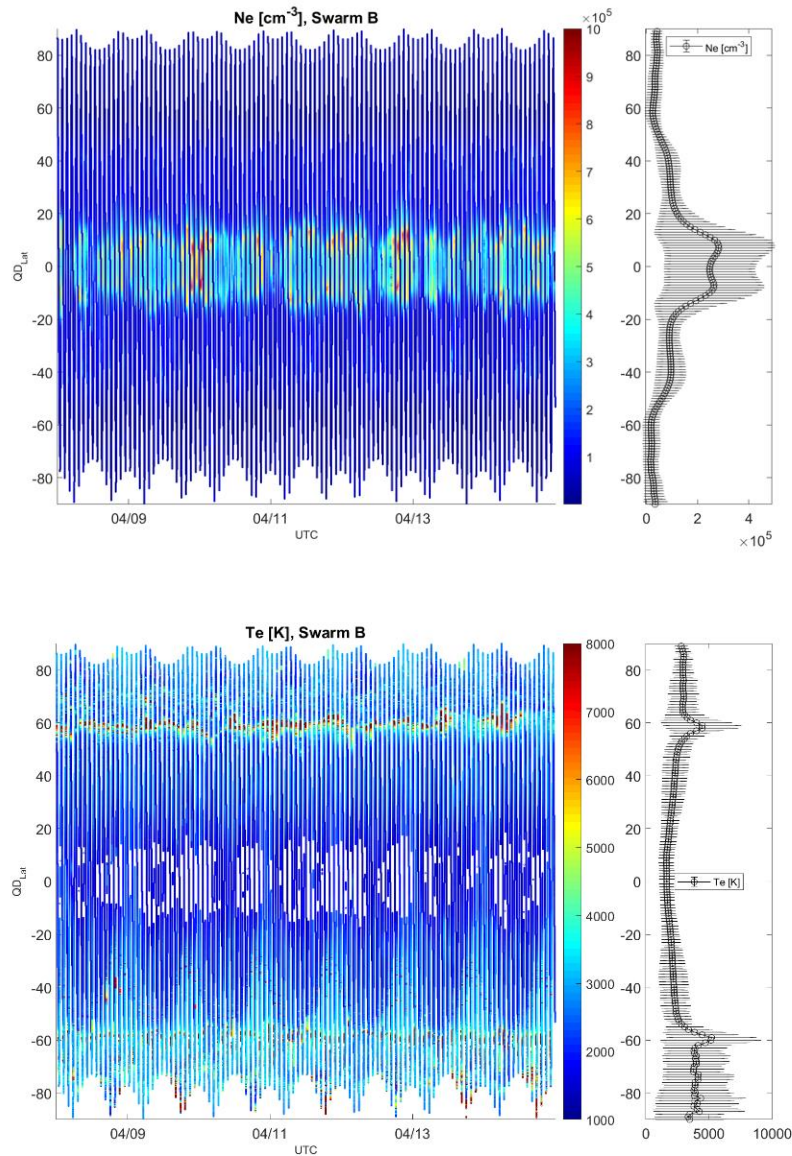


Figure 6-5 :

Plasma density (upper panel) and electron temperature (bottom panel) measured on board Swarm Bravo between the 8th and the 15th of March 2018, as a function on Latitude in quasi dipole coordinate and time. The vertical lateral panel shows the average (squares) and standard deviation (vertical bars) for each degree in latitude.

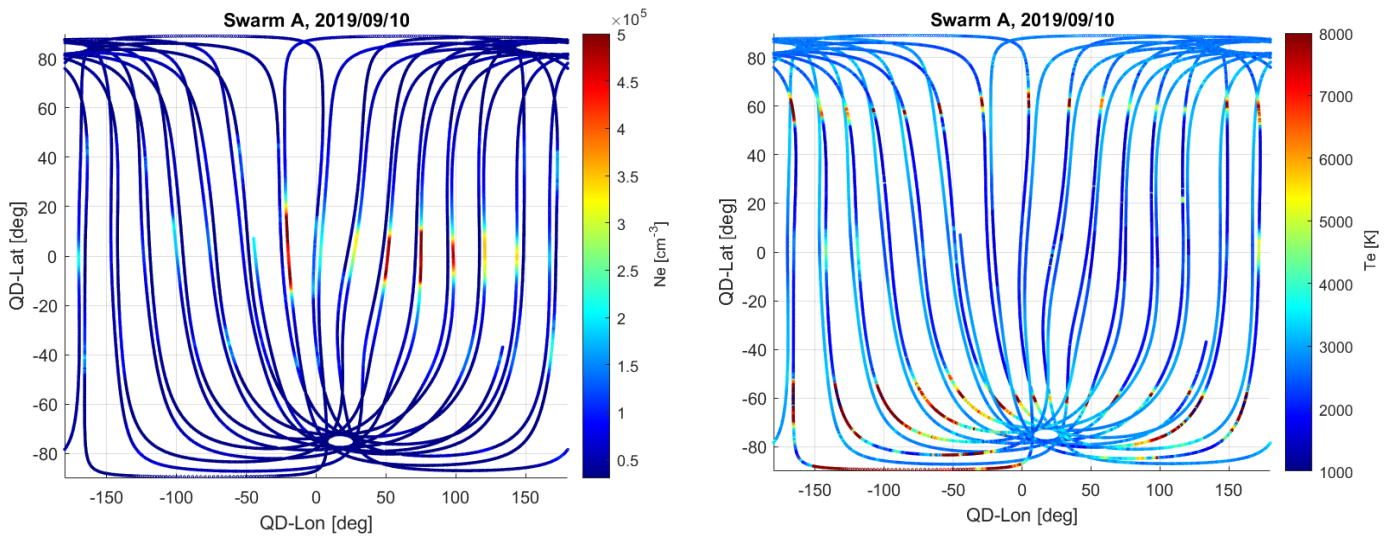


Figure 6-6 :

Daily variation of density (left panel) and electron temperature (right panel) as a function of latitude and longitude in quasi dipole coordinate system, measured on board Swarm Alpha on the 10th of September 2019.

6.2 New baseline achievements

Currently, the EFix_LP_1B data products have Product Baseline 05 and File Counter 01. Each time that a new change in the algorithm processor is introduced, the baseline is incremented. The last modification of the plasma algorithm was introduced with the full reprocessing campaign in the 2018. For a detailed description of the improvements introduced in the Swarm operation processors it is possible to refer to [RD.1]. In particular, for the plasma processor, there are two major evolutions that are worth to be mentioned also in the present document:

- A new LP product interpolated at exact UTC has been introduced and it is named EFixLPI_1B
- The electron temperature T_e is now mainly computed from the high gain probe

In the following those two are discussed in more details.

6.2.1 New LP product interpolated at exact UTC

The EFix_LP_1B data products have the samples at 2Hz LP timestamp, while the EFixLPI_1B data products contain the samples interpolated at exact UTC, thus 1Hz data cadence. These interpolated products are aligned, with the magnetic field data at 1Hz rate (i.e., MAGx_LR_1B) facilitating multi-sensor joint scientific investigations.

Figure 6-7 shows density and electron temperature time series measured on board Swarm Bravo on the 27th of April 2017, black lines represent the measurements at LP timestamp stored in EFix_LP_1B data products, while red lines represent the interpolated measurements at exact UTC stored in the EFixLPI_1B data products. The differences between both data sets are hardly noticeable for the densities, and visible, but small, for the electron temperature. The differences are due both to the fluctuating nature of T_e , and to interpolation artefacts reducing the number of samples for the interpolated products. However, the EFixLPI_1B dataset can be considered to have a similar in quality as the data at LP timestamps.

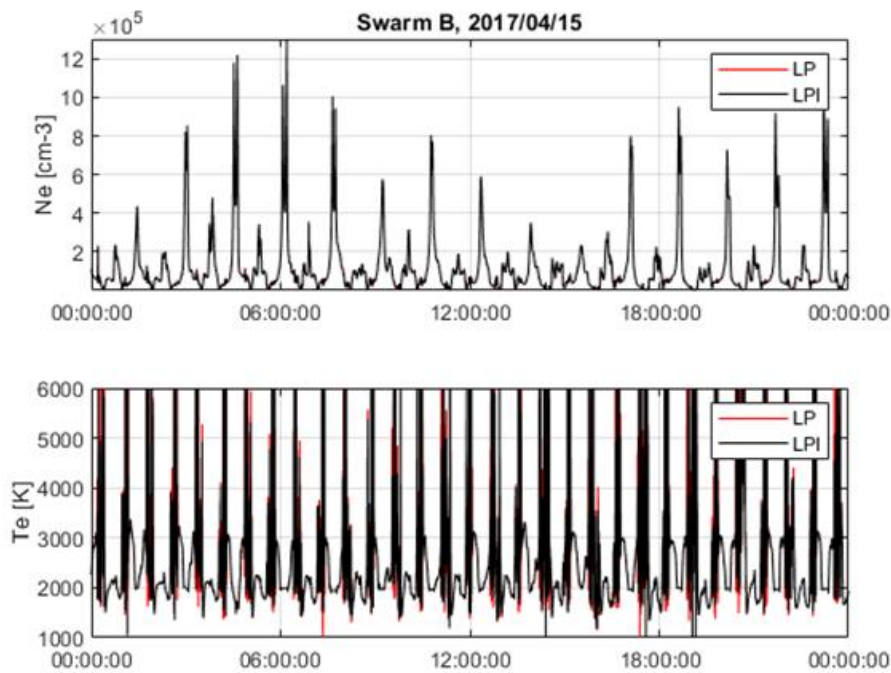


Figure 6-7 :

Density and electron temperature time series (upper and bottom panel, respectively) measured on board Swarm Bravo on the 27th of April 2017.

The black lines represent the EFix_LP_1B data products, while red lines represent the EFixLPI_1B data products.

6.2.2 Te computed from high gain probe

Previous L1B algorithm estimated electron temperature by using three possible methods: from the high gain probe for low electron density (below a low threshold); from the low gain probe for high electron density (above a high threshold); as a blended value with a linear weighting between the two probes for intermediate values of electron density. However, temperatures from the two probes were systematically different from each other causing discontinuous jumps or artificial variations at transitions between low and high densities caused by blending. It was then proposed to derive temperature only from one probe, using the one set to high gain which is less noisy, less biased and seems to be valid even when overflows are detected. In very few cases the low gain measurements are used when the high gain data are flagged with errors. Figure 6-8 shows the density and electron temperature stored in the EFix_LP_1B data products (or latest baseline, red lines) and the one stored in the EFix_PL_1B data products (or older baseline, black lines) measured on board Swarm Alpha on 1st of January 2018. The bottom panels show the same variables in a smaller interval of time. It is possible to observe that the electron density computation has not changed, as expected, because no changes have been introduced in the algorithm for the computation of this variable.

While, as mentioned above, with the new baseline the electron temperature is derived only from the high gain probe measurements. The data from the high gain probe are observed to be more stable in region of low density. However, the detected ADC overflow for high densities typically at the dayside equator crossing regularly leads to flagged temperatures. These characteristics are visible in the bottom side of Figure 6-8, where data are

shown for few spacecraft orbits, evidencing the regions of low and high density where T_e derived from the latest baseline (red lines) is more stable with respect to the one of the older baseline (black lines).

Finally, Figure 6-9 shows the difference of T_e as stored in the latest baseline and the older baseline, as a function of the Latitude. The largest differences between the two are observed at higher latitudes, where the density is generally lower and the temperature is characterized by fluctuations.

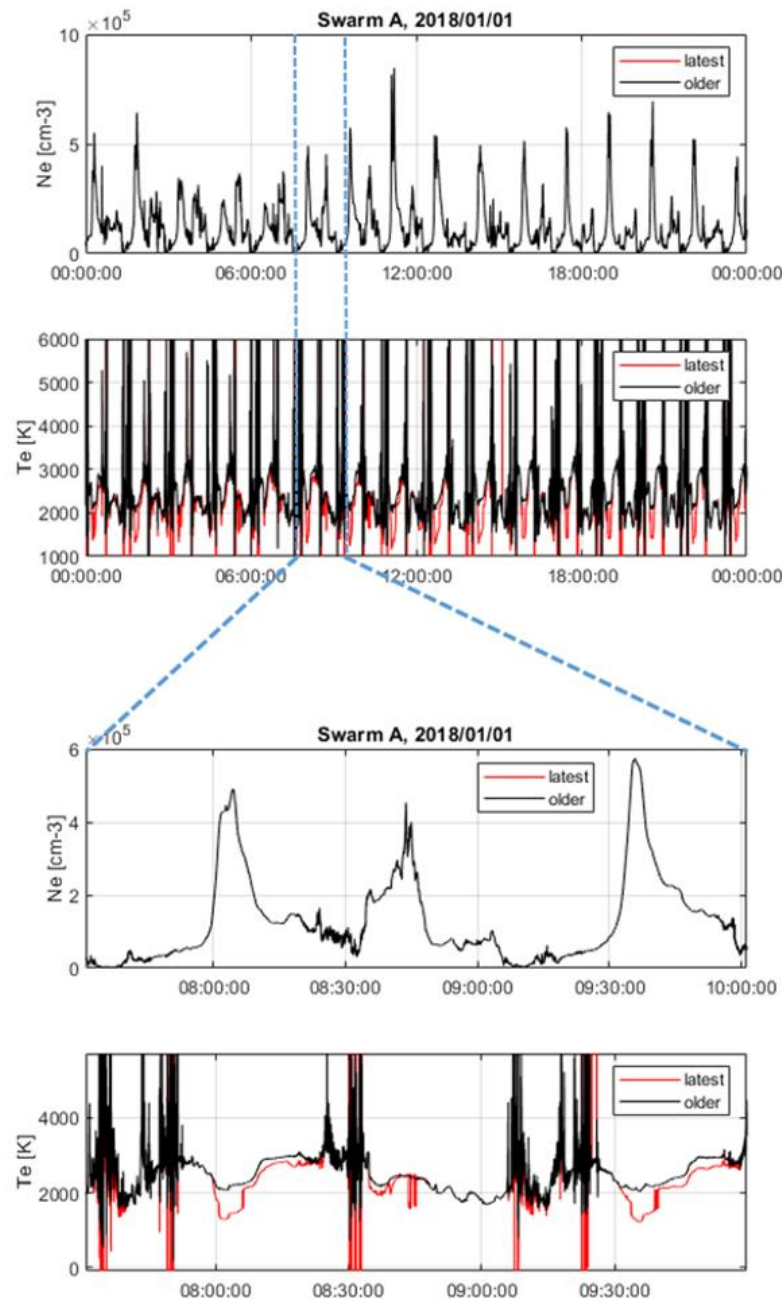


Figure 6-8 :

Time series of Ne and T_e derived from the EFix_LP_1B products (or latest baseline, red lines) and from the EFix_PL_1B products (or older baseline, black lines) measured on board Swarm Alpha for the day January 1st, 2018. The bottom panel reproduced a smaller interval of time. Both flagged and nominal data are shown.

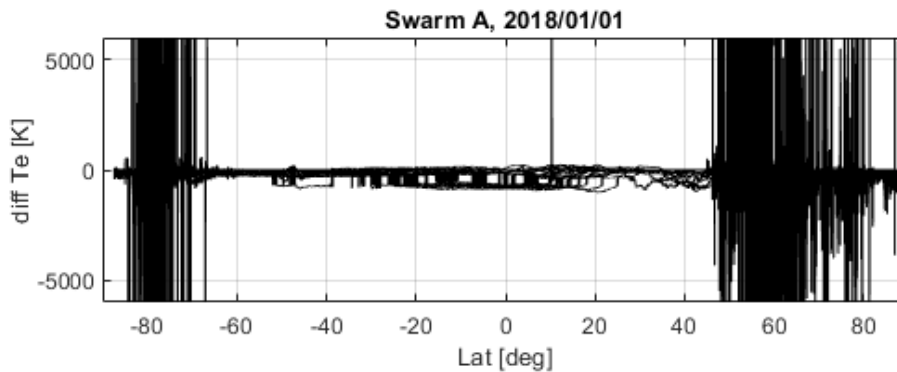


Figure 6-9 :

Differences of electron temperature derived from the EFlx_LP_1B products (or latest baseline) and from the EFlx_PL_1B products (or older baseline) measured on board Swarm Alpha for the day January 1st, 2018.

6.3 Recent tests performed on the LPs

Several in-flight tests have been performed on the LP since the launch of the mission, with the objective to further improve the performance of the instrument and study the effect on the measurements. In this document are reported only recent tests implying major impact on the plasma data quality.

6.3.1 Both probes set in high/high gain

During two weeks in July 2019, both the LP probes on board Swarm Alpha have been set in high gain mode from the 8th of July 2019 at 00:00 UTC to the 22nd of July 2019 at 00:00 UTC. During this period, also a specific setting for zero tracking harmonic mode has been tested. The scopes of this test period was to optimize the instrument settings during the nominal operation mode.

The impact of the high/high (h/h) mode on the data quality differs depending on the variables. Figure 6-10 shows the daily average of density, electron temperature (left panel, black and blue lines respectively) and spacecraft potential (right panel). The data are shown from the 4th to the 29th of July 2019, as measured on board Swarm Alpha. The shadowed regions in Figure 6-10 denote the period of h/h gain mode for the LPs.

From the left panel it is possible to observe a jump in the measurements on 10th July, just after the LP change setting. While no variations are observed on the 9th and the 23rd of July, corresponding to the start and end days of the h/h test. Thus, it is possible to assume that the jump on the 10th of July is not due to the h/h mode, but it is most probably related to a weak geomagnetic activity observed in that day [RD.16]. As a consequence, the general trend of Ne and Te is not changed due to the period on h/h gain mode. This is related to the fact that these two variables are computed from the probe in high gain mode only, thus the h/h test has no impact on their computation. Considering the right panel in Figure 6-10, it is possible to observe how this test affects the computation of the spacecraft potential. This variable, is generally computed from the probe in low gain mode, thus in the shadowed region is showing Vs as computed from the probe in high gain mode. Vs is larger when

derived from the high gain probe, with an average difference of about 1.5 V with respect to the measurements from the low gain. This result is as expected, since the gain setting is basically increasing the value of the resistor.

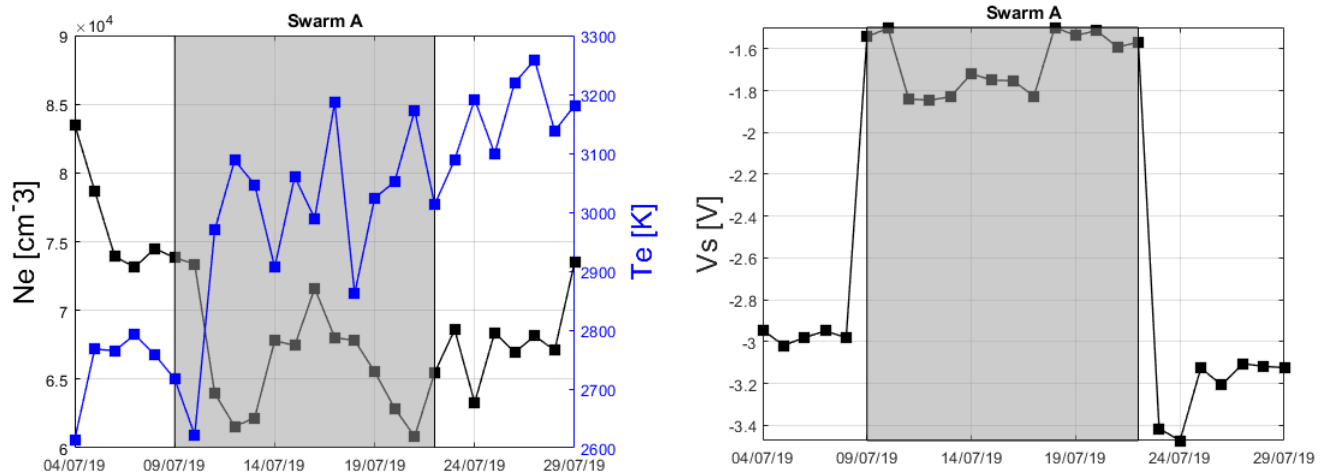


Figure 6-10 :

Daily average (squares) of Ne, Te and Vs (left and right panels, respectively) measured on board Swarm Alpha between the 7th and the 29th of July 2019. The shadowed area denotes the period when both the probes were set to high gain mode.

6.3.2 Swap of LP gain setting

At the beginning of the mission the initial setting was the Probe 1 in low gain mode and the Probe 2 in high gain mode. The two probes are made of nitrated titanium (TiN), but Probe 2 is covered with gold (Au). In December 2018 the probe settings have been swapped, thus currently Probe 1 is in high gain mode and Probe 2 is in low gain mode. The swap of the gain mode setting was performed on all the Swarm spacecraft, in particular on the 14th of December for Alpha and Bravo, and on the 16th for Charlie. This test did not impact the quality of Ne and Te, but had impact on the computation of the Vs.

Left panels in Figure 6-11 show the Ne, Te and Vs measured on board Swarm Alpha between the 15th and 17th of December 2018. There is not a visible change for the Ne and Te variables, while around the 16th of December the Vs measurements become weaker and show a decreasing trend. The right side of Figure 6-11 shows the daily average of the Vs (green squares) together with the standard deviation (vertical bars) from January 2014 to January 2019. It is possible to notice that in correspondence of the date of the LP swap, the Vs average value decreases of about 1.5 V with respect to the previous period. This difference is introduced with the swap of the LP settings, and it is possibly related to the difference in the material covering the probes. However, further investigations are needed to gain more insights this impact on the Vs measurements. The same analysis has been performed both for Te and Ne variables (see for example Figure 6-1 (a) and (b)), and the results demonstrated the these two variables have been not impacted by the LP setting swap.

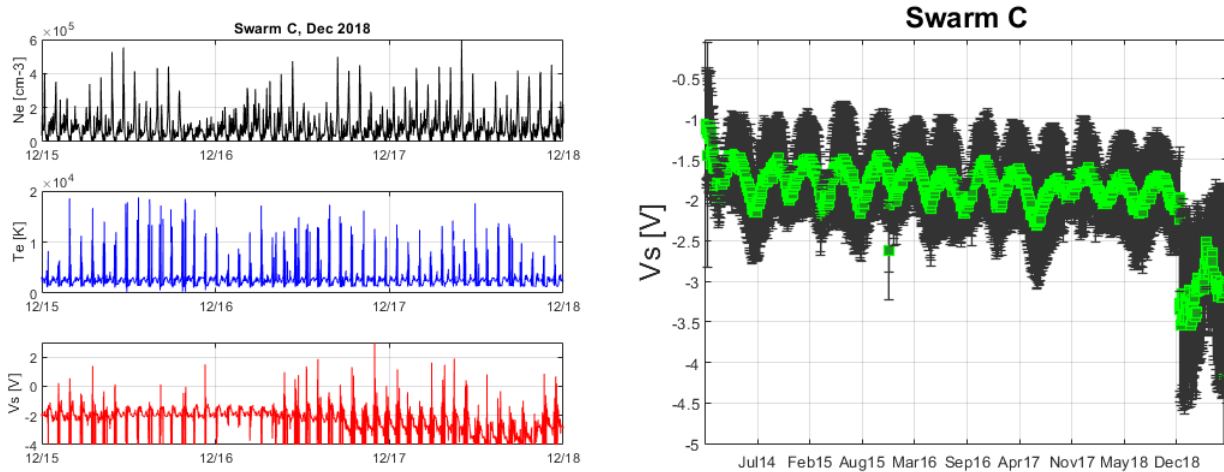


Figure 6-11 :

The left figure shows a time series of Ne, Te, and Vs measured on board Swarm Charlie between the 15th and the 17th of December 2018. The right figure shows the daily average (green squares) and standard deviation (vertical bars) of the Vs measured on board Swarm Charlie between January 2014 and June 2019.

6.4 On-going investigations and expected improvements

The good quality of the LP data has been discussed in the previous sections, demonstrating that the Swarm EFI-LP data products are able to capture and characterize the main features of the ionospheric plasma. Also, from a data quality point of view, some improvements have been introduced with the last processing baseline [RD.1] and continuous tests are performed to further enhance the instrument performance.

However, some anomalies have been identified, affecting the LP data. Unfortunately, these anomalies impact the quality of level 1B data and there is not a proper solution yet. Further investigations are ongoing with the aim to get more on the nature of these anomalies and on possible workaround to improve the data quality.

In the following a short description of some anomalies is given.

6.4.1 Extreme values of the electron temperature

The electron temperature has typical values in the ionosphere ranging from few hundred of Kelvin during quiet period at lower latitudes, up to few thousand of Kelvin reaching peak of 8000 K during extreme events as, for example, the STEVE [RD.17]. However, Swarm measures Te up to more than ten thousand of Kelvin, suggesting that some of these extreme values is more related to instrumental issues than physical processes. Numerous investigations are ongoing in order to identify the source of these high Te values, which more frequently occur in the southern hemisphere and are distributed respect to particular angles between the sun illumination and the spacecraft orientation.

6.4.2 LP difference

Between the two probes, it is expected to observe a potential difference related the term $\mathbf{v} \times \mathbf{B}$, where \mathbf{v} is the particle velocity, and \mathbf{B} is the electric field. Such difference is expected to be around 115 mV, while from the analysis it is observed to have a potential difference of 1.5 V, quite larger than the predicted value. The issue is

currently under investigation but, since a preferential probe is used to compute the LP L1B data, it has no impact on the data quality.

6.4.3 Hick-ups

The periodic passage from harmonic submode to sweep mode, actually represent a discontinuity in the data acquisition method. Indeed, it is often observed the presence of hick-ups in LP L1B data products. These consists in small fluctuations of T_e and V_s in correspondence of the sweeps mode. The investigation is on-going aiming to identify an automatic procedure to easily filtered out these small jumps.

6.4.4 Ne fluctuations

Systematic small amplitude Ne fluctuations are observed during dayside orbits. These fluctuations are more probably related to instrumental issues, since they are not observed when computing Ne from the face plate measurements. A statistical classification of these is being performed, in order to add a flag identifying this disturbance in the LP L1B data products

7 ACCELE L1B Data Products

The accelerometer L1B data contains the raw accelerometer measurements, which were converted into physical units. No other processing or correction is applied in the L1B processing because the accelerometer measurements are heavily perturbed by a variety of artefacts to an extent, where an automated, unsupervised correction is not possible [RD.18]. Therefore, the artefacts with the largest negative impact on data quality are corrected in the L2 processing, where an operator supervises the correction process and performs part of the corrections manually. The L2 accelerometer data product is constructed such that it is possible to revert all applied corrections, thereby restoring the raw measurements, which are otherwise not provided to Swarm users [RD.19]. In the following is provided an overview of the known artefacts in the accelerometer measurements and comment on the correction process.

7.1 Temperature-induced bias variations

The bias of the accelerometers is extremely sensitive to temperature changes. This is illustrated in Figure 7-1 for the Swarm C satellite, where a heater was activated on the 16th of January 2014 to increase the temperature of the accelerometer by 4°C, which resulted in a change of the accelerometer bias of 10^{-5} m/s². This change in bias is 100 times larger than the non-gravitational acceleration signal.

The most accepted hypothesis is that a residual capacitance of the brass wall stops, which changes with temperature, is causing this artefact. Six thermistors are intended to measure the temperature of the accelerometer mechanical sensor structure. However, the thermistors are placed on the electronic boards surrounding the mechanical sensor structure. The time lag between a temperature change measured by the thermistors and felt by the inner parts of the sensor structure is approximately 30 minutes. In reality, the situation is more complex requiring a dedicated model for the heat transport from the thermistors to the sensor structure, noting that the heaters are not placed all around the sensor, but only on three sides.

In the L2 processing, a simplified model of the heat transport removes the largest part of the temperature-induced bias variations. Remaining effects are removed in the fusion of the accelerometer measurements with the GPS receiver-derived non-gravitational accelerations, which is also part of the L2 processing.

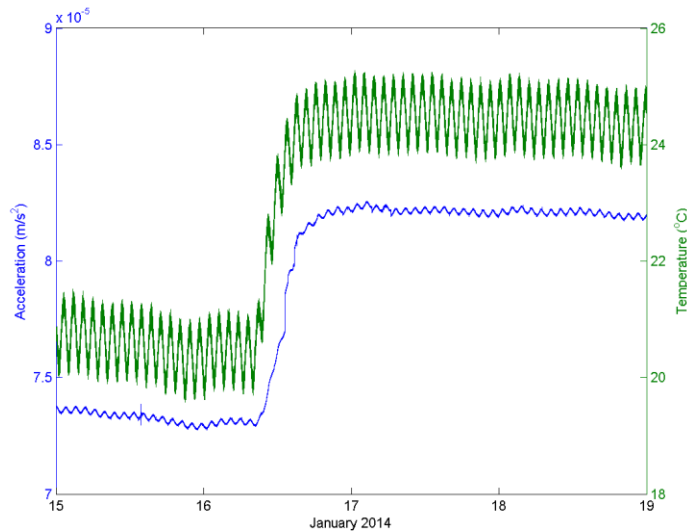


Figure 7-1:

Temperature-induced bias variations illustrated for the Swarm C accelerometer.

7.2 Sudden changes of the bias (steps)

The accelerometer measurements contain a large number of unpredictable changes in the bias, which can be roughly divided into two categories:

1. Sudden, large bias changes, which are often accompanied with signs of micro-seismic
2. Repeated changes of the accelerometer bias.

The first category could be caused by a sudden mechanical adjustment of the accelerometer sensor structure in response to thermal stress or by the proof mass settling into another stable position, where the change was triggered by a micro-seismic event on board of the satellite. An example of such a step is presented in Figure 7-2 in the left panel. A typical feature of the second category is that the bias appears to change several times per orbital revolution, and that it alternates between two or more levels. The right panel of Figure 7-2 gives an example where the bias alternates between five levels. The repeated steps occur often on time scales of several days to weeks.

All sudden steps are corrected in a two-stage procedure in the L2 processing. The first stage is an automatic step correction that is able to detect and correct 80% of all steps. The second stage is a visual inspection of the accelerometer data and manual correction of all remaining steps.

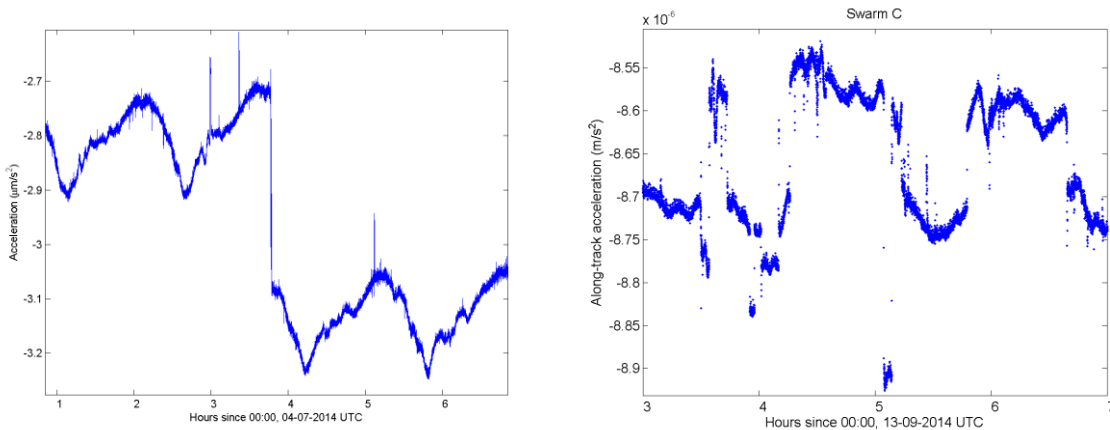


Figure 7-2:

Sudden, large changes (left panel) and repeated changes (right panel) of the accelerometer bias.

7.3 Slow changes of the bias (silent steps)

In rare cases, the accelerometers bias changes slowly over a few hours to a different level. A typical example is illustrated in Figure 7-3. Though it is not clear what causes such changes, there is no indication that they are related to temperature changes.

The slow changes of the accelerometer biases are removed to a large extent in the fusion of the accelerometer measurements with the GPS receiver-derived non-gravitational accelerations, which is also part of the L2 processing.

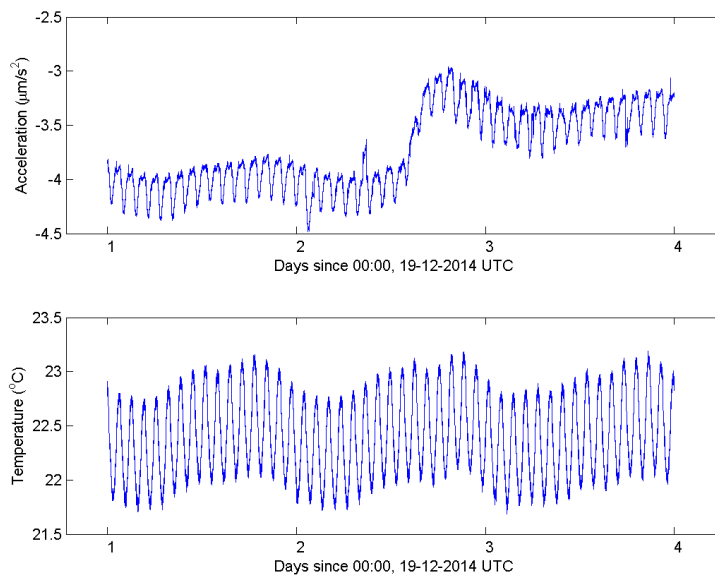


Figure 7-3:

Change of the accelerometer bias the slowly occurred over a period of a few hours (top panel) and is not related to temperature changes (bottom panel).

7.4 Autonomous reboot of the accelerometer

Approximately once per month the Error Detection And Correction (EDAC) device on board the Swarm spacecraft, reports an error in the memory of the accelerometers and get stuck in an infinite loop. In order to recover fast from this situation, the on board computer detects such EDAC events and automatically triggers a reboot of the accelerometer, which fixes the issue. This results in a data gap of 3 minutes and 18 seconds. A side effect is that the accelerometer temperature slightly drop during the reboot since the accelerometer electronics are switched off for a short time, during which they produce no heat. As a consequence, a large change of the bias and a high number of sudden bias changes (steps) occur during the next few hours after an EDAC event. Since EDAC events cause data gaps of a specific duration, they are easy to detect. The next three hours after an EDAC event are flagged as invalid data.

7.5 Sudden changes in sensitivity

In rare cases, the sensitivity of the accelerometer measurements to temperature variations changes within an instant. This can be the case at large, sudden steps as shown in Figure 7-4 or, potentially, after a reboot of the instrument.

The calibration of the accelerometer measurements, which is part of the L2 processing, is performed in batches of several months. The start and end of each batch is carefully selected after visual inspection of the accelerometer measurements. The batches are selected such that one set of calibration parameters is valid for each batch. In the example illustrated in Figure 7-4 the start/end of such batches would be in the centre of the figure, where the large sudden step occurs approximately at 4:20 on the 7th of August 2015.

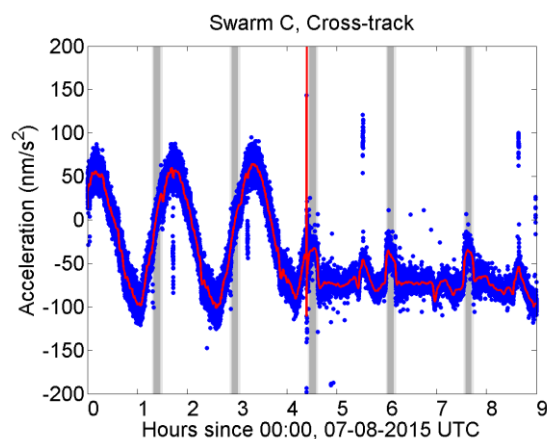


Figure 7-4:

Sudden, dramatic change in the sensitivity of the Swarm C cross-track accelerations to temperature variations, which occurred at a large step (corrected in the figure) on the 7th of August 2015.

7.6 Pink noise

The accelerometer measurements contain random noise with a power spectral density (PSD) that is reciprocal to the frequency, whereas prior to launch the PSD was specified to be flat in the frequency range from 0.1 mHz

to 1 Hz. The PSD of the along-track measurements of the Swarm A, B and C accelerometers are presented in Figure 7-5. Since the noise is random, no correction is possible.

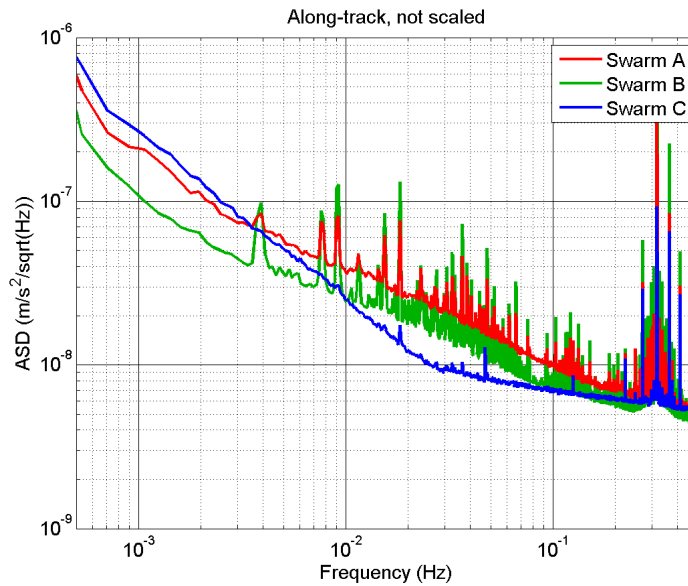


Figure 7-5:

Sudden, dramatic change in the sensitivity of the Swarm C cross-track accelerations to temperature variations, which occurred at a large step (corrected in the figure) on 7th of August 2015.

7.7 Non-unit scale factors

The accelerometer scale factors, which are related to an imperfect conversion of the control voltages to the accelerations in physical units, should nominally be close to one, where the imperfection should be in the order of a few percent. However, the scale factors deviate by several hundreds of percent from the nominal value, which is not understood.

Several satellite manoeuvres were designed, in which the attitude thrusters were activated in a special sequence that did not alter the orbit, but created a marked signal that was within the dynamic range of the accelerometers. It is assumed that the thrust forces are known with an accuracy of 5% or better, allowing the scale factor to be estimated with that accuracy. Figure 7-6 shows the accelerometer measurements during a manoeuvre for the along-track accelerometer measurements of the Swarm C satellite. The accelerometer measured a peak-to-peak amplitude of 74.9 $\mu\text{m/s}^2$, whereas the thrusters were known to produce an acceleration of 92.3 $\mu\text{m/s}^2$, inferred from the sum of the nominal thrust force vectors and the satellite mass. Thus, the acceleration measurements need to be scaled by a factor of 1.23 to match the thrust.

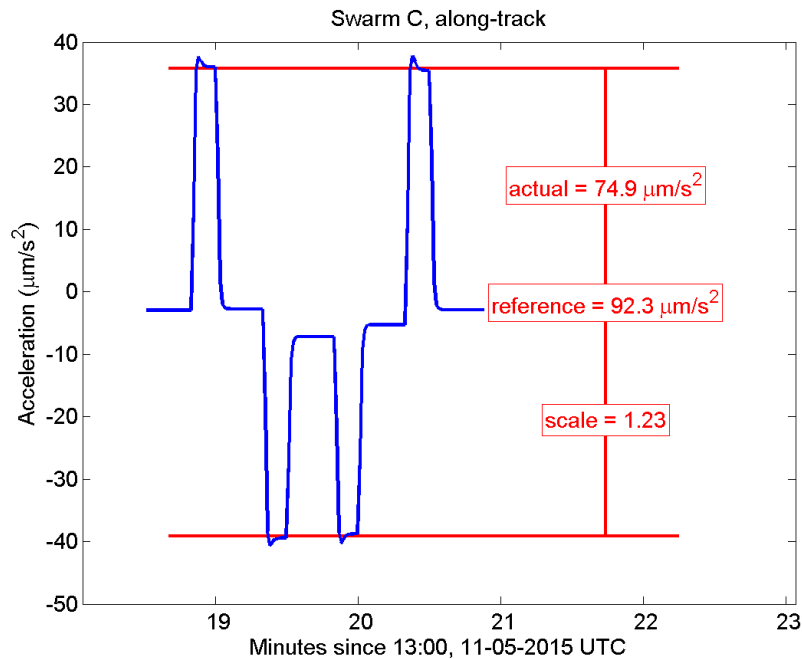


Figure 7-6:

Accelerometer measurements during an accelerometer scale factor calibration manoeuvre.

Dedicated manoeuvres were performed for all three satellites and all three accelerometer axes. For the cross-track axis two different thruster activation sequences were performed. The results for the scale factors are summarized in Table 1. When these scale factors are applied, the accelerometer measurements of the three satellites appear to be consistent in scale. This is demonstrated in Figure 7-7, which shows the Swarm A and C along-track measurements during a small geomagnetic storm on the 8th of June 2014 without and with applying scale factors (left and right panel, respectively). Clearly, the peak acceleration a 6:50 has the size once the scale factors are applied. The scale factors that were estimated from the dedicated manoeuvres are applied in the L2 processing.

	Swarm A	Swarm B	Swarm C
Along-track	2.18	3.63	1.37
Cross-track (option 1)	1.59	2.03	1.14
Cross-track (option 2)	1.82	2.39	1.13
Radial	1.59	6.66	1.08

Table 1:

Scale factors estimated from dedicated satellite manoeuvres.

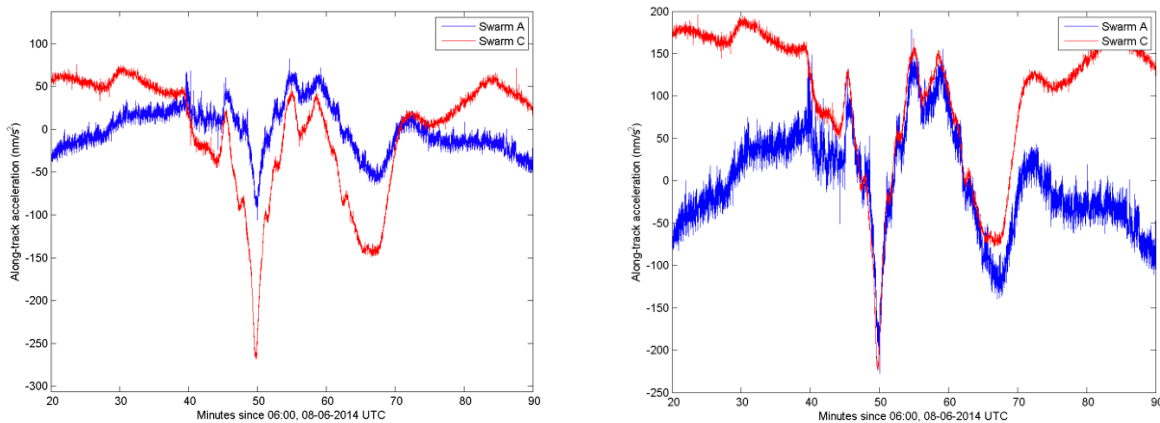


Figure 7-7:

Swarm A and C accelerometer measurements before (left) and after (right) applying scale factors that were estimated from dedicated calibration manoeuvres. Measurements were taken during a small geomagnetic storm on the 8th of June 2014. The measurements are not corrected for temperature-induced bias variations.

7.8 Spikes

The accelerometer data contains a large number of artificial spikes, whose origin is not clear. The spikes occur in sequences of 10–20 spikes, where each spike has a duration of several tens of seconds, a size of a few tens to a few hundreds of nm/s^2 , and a distance to the next spike of 1–3 minutes. When spikes are perturbing the measurements, typically two such sequences occur per orbital revolution. Figure 7-8 presents a typical sequence of spikes.

Spikes are automatically detected in an automatic procedure of the L2 processing. The affected measurements are replaced by linear interpolation of the surrounding healthy measurements and flagged as invalid data.

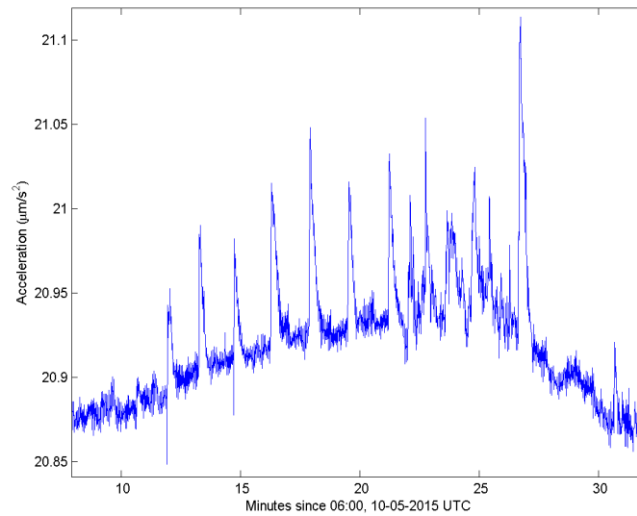


Figure 7-8:

Spike sequence in the along-track accelerometer measurements of Swarm A.

7.9 Harmonic perturbations

The accelerometer measurements are superimposed with harmonic perturbations. One such perturbation is believed to originate from aliasing from an unknown high-frequency artificial signal. The main aliasing frequency is at approximately 0.3 Hz, with multiple harmonics as illustrated in Figure 7-9. There exists a second harmonic signal with a period of 2800 seconds of unknown origin, which is highlighted in the spectrogram in Figure 7-10.

A prototype of a harmonic resonator was developed, which is capable of removing the harmonic perturbations when no spikes are present. Since the accelerometer measurements are increasingly affected by spikes, the harmonic resonator is not applied. The L2 accelerometer data thus contain the harmonic perturbations. However, these are fairly small for the Swarm C satellite.

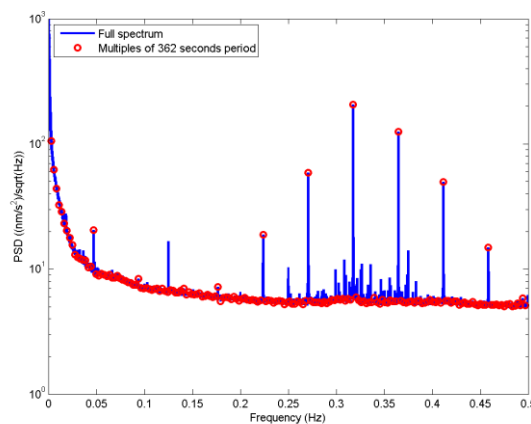


Figure 7-9:

PSD of the along-track accelerometer measurements of Swarm C.

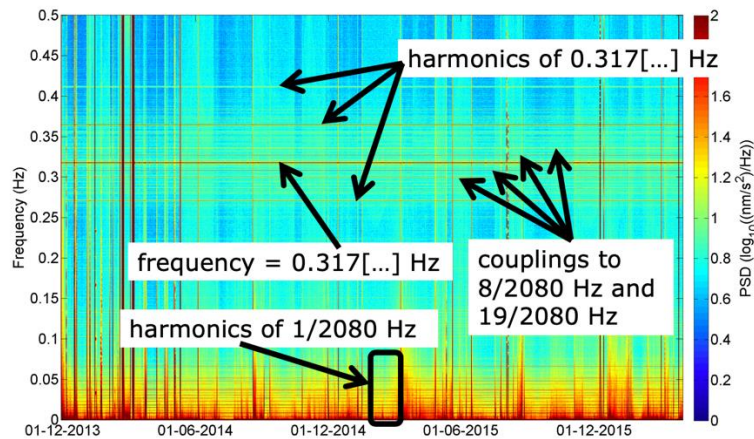


Figure 7-10:

Spectrogram of the along-track accelerometer measurements of Swarm C.

7.10 Polarization voltage perturbations

The acceleration measurements are superimposed with a small perturbation of up to 10 nm/s^2 , which correlated with variations of the polarization voltage. Unfortunately, the polarization voltage is measured only every two seconds (data rate is 1 Hz, but every second sample is simply repeated). Therefore, the positive and negative LTC voltages are presented instead in Figure 7-11. The size of the variations in the polarization voltage correlates with temperature variations, which can however suddenly change at EDAC events. This correlation is demonstrated in Figure 7-12.

Due to the small impact on the accelerometer measurements and problems in reliably removing the effect, no correction is applied in the L2 processing.

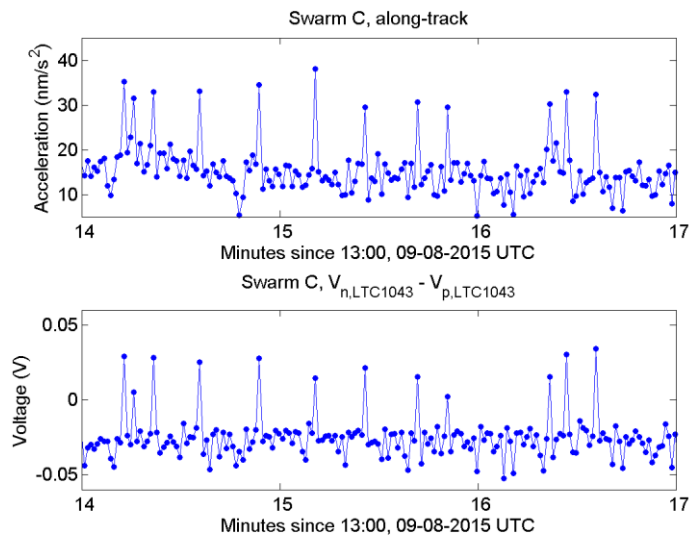


Figure 7-11:

Small variations in the accelerometer measurements (top panel), which correlate with variations in the polarization voltage (bottom panel).

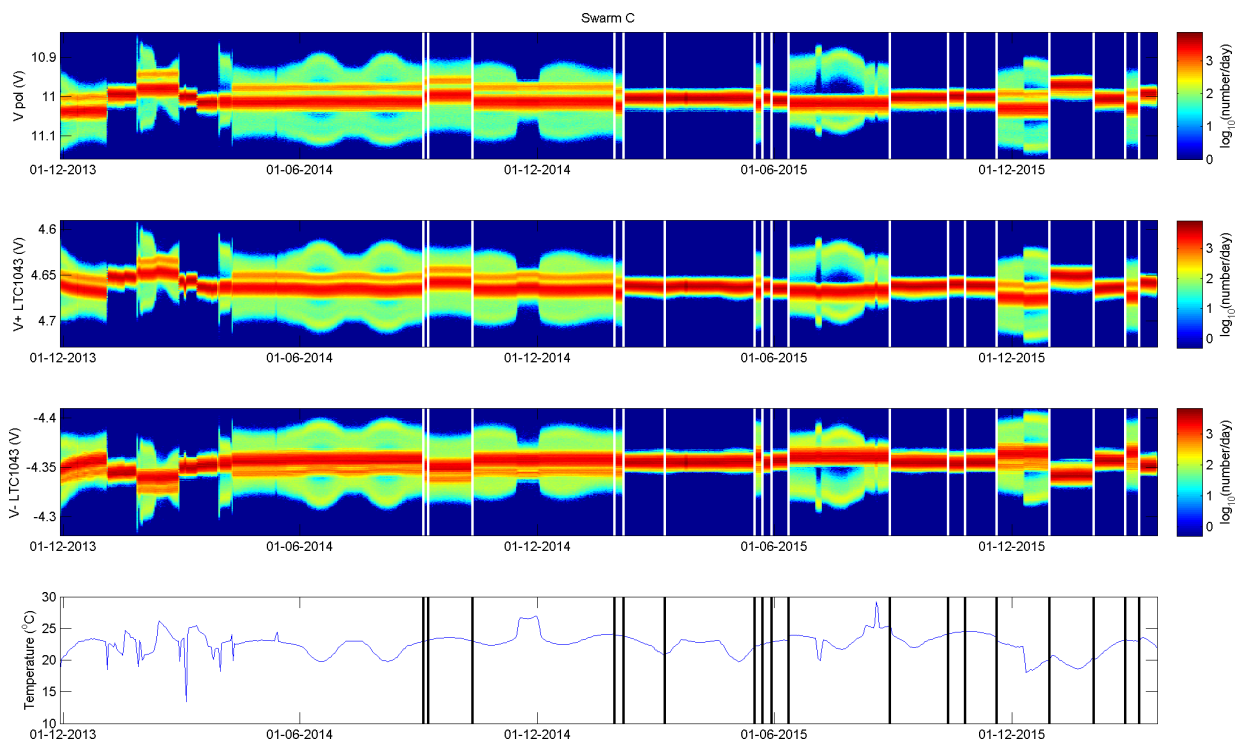


Figure 7-12:

Temperature-induced variations in the polarization voltage.

7.11 Coupling between accelerometer axes

The accelerometer axes are supposed to provide independent measurements. In reality, the Swarm accelerometers show couplings between axes up to 30%, which is most apparent during the calibration manoeuvres. Figure 7-13 shows the three linear acceleration measurements during an accelerometer scale factor calibration manoeuvre, where thrust was exerted only in the along-track direction. Clearly, the cross-track and radial accelerations show the same signal as the along-track direction, even though there was no thrust into these directions. These couplings are not well understood.

No correction is applied in the L2 processing. Since in a nominal satellite attitude the largest signal is measured by the along-track axis, we expect a larger perturbation in the cross- and radial axes, and only a smaller perturbation vice versa.

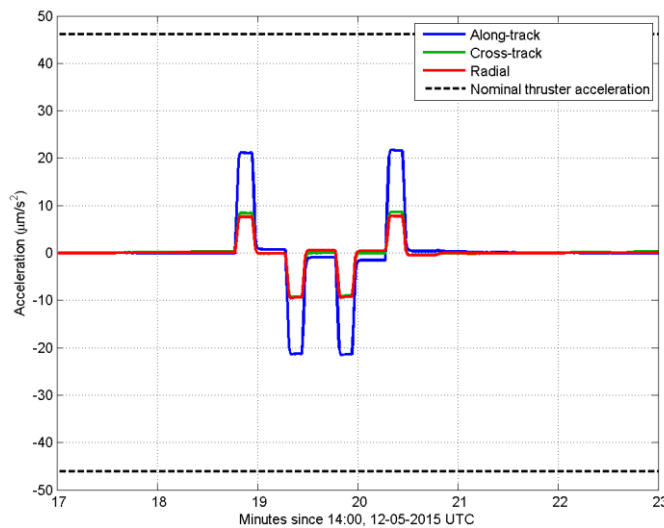


Figure 7-13:

Coupling between accelerometer axes for the Swarm C accelerometer. A strong linear acceleration was created by the thrusters only in the along-track direction.

7.12 Summary and perspective

The accelerometer data contains a large number of perturbations, which are described in the sections above. Extensive investigations, in which ESA has collaborated with partners in industry and science, resulted in a number of well-justified hypotheses on the root causes of the perturbations. However, since there is hardly any instrument setting that can be changed, it is the general consensus that there is no possibility to conduct further experiments on board of the satellite in search of the root causes of the perturbations. This implies that there is no possibility to prevent that perturbations occur. As a consequence, a lot of effort was invested into detecting and correcting the perturbations in the Level 2 processing of the accelerometer data, where an operator supervises the partly automated processing. Currently, corrections for the non-unit scale-factors, temperature-induced bias fluctuations, sudden steps, and spikes are implemented and applied in the Level 2 processing. Recently, it became apparent that a correction for the coupling between accelerometer axes is needed. In the future, we will continue our efforts to further improve the capabilities of the accelerometer data processing system, enabling us to provide more and better calibrated accelerometer data to Swarm users. This includes make existing corrections more reliable as well as implementing new corrections to known perturbations.